Collagen VII plays a dual role in wound healing

Alexander Nyström,[1] Daniela Velati,[1] Venugopal R. Mittapalli,[1] Anja Fritsch,[1] Johannes S. Kern,[1] and Leena Bruckner-Tuderman[1,2]

[1]Department of Dermatology, University Medical Center, Freiburg, Germany. [2]Freiburg Institute for Advanced Studies, School of Life Sciences — LifeNet, Freiburg, Germany.

Although a host of intracellular signals is known to contribute to wound healing, the role of the cell microenvironment in tissue repair remains elusive. Here we employed 2 different mouse models of genetic skin fragility to assess the role of the basement membrane protein collagen VII (COL7A1) in wound healing. COL7A1 secures the attachment of the epidermis to the dermis, and its mutations cause a human skin fragility disorder coined recessive dystrophic epidermolysis bullosa (RDEB) that is associated with a constant wound burden. We show that COL7A1 is instrumental for skin wound closure by 2 interconnected mechanisms. First, COL7A1 was required for re-epithelialization through organization of laminin-332 at the dermal-epidermal junction. Its loss perturbs laminin-332 organization during wound healing, which in turn abrogates strictly polarized expression of integrin α6β4 in basal keratinocytes and negatively impacts the laminin-332/integrin α6β4 signaling axis guiding keratinocyte migration. Second, COL7A1 supported dermal fibroblast migration and regulates their cytokine production in the granulation tissue. These findings, which were validated in human wounds, identify COL7A1 as a critical player in physiological wound healing in humans and mice and may facilitate development of therapeutic strategies not only for RDEB, but also for other chronic wounds.

Introduction

Impaired cutaneous wound healing is a complication of many major diseases; consequently, chronic wounds confer a high socioeconomic burden for the society (1). Therapeutic intervention is possible only to a certain degree, since the pathogenetic mechanisms underlying delayed wound closure are not fully understood. After acute tissue injury, wound healing proceeds as a highly orchestrated process in 3 overlapping phases (2, 3). First, directly after wounding, activated thrombocytes form a fibrin clot to stop bleeding and to maintain tissue homeostasis; this is accompanied by recruitment of neutrophils and macrophages by proinflammatory cytokines released into the injured tissue (3, 4). The second phase aims at repair of the wounded area. Recruited blood cells stimulate keratinocytes to proliferate and migrate to cover the wound. In the dermis, the fibrin clot is replaced by a vessel- and collagen-rich granulation tissue, in which the fibroblasts differentiate into myofibroblasts that contract the wound (3). The third and longest phase of wound healing includes maturation and remodeling of the new tissue. In this phase, myofibroblasts and excessive capillaries disappear, and tissue strength is improved by turnover and remodeling of the provisional extracellular matrix (3).

As an organ that is constantly exposed to external dangers, the skin requires mechanical toughness and efficient repair mechanisms. Maintenance of integrity and resistance to frictional forces are provided by the interface between the epidermis and the dermis, the dermal-epidermal junction zone (DEJZ) (5, 6). Loss-of-function mutations in the genes encoding DEJZ proteins are responsible for skin fragility disorders collectively termed epidermolysis bullosa (EB), which manifest with mechanically induced skin blisters and chronic skin fragility (7). This proves the importance of the DEJZ and its individual components for preservation of skin integrity.

However, knowledge of the role of individual DEJZ molecules in wound healing remains limited. To migrate over the granulation tissue, keratinocytes use β1 integrins, which interact with fibrinogen, fibronectin, and collagens abundant in the provisional extracellular matrix. The cells further back from the epidermal leading edge deposit laminin-332 into the provisional extracellular matrix and switch to expression of integrin α6β4. The laminin-332/integrin α6β4 interaction is believed to support directed migration of keratinocytes (8), since integrin α6β4 regulates front-rear polarity of keratinocytes through activation of Rac (9–11). Laminin-332/integrin α6β4 interaction is also required for reassembly of the DEJZ, reformation of hemidesmosomes, and stable epidermis (8, 12).

Beyond the integrin-laminin interactions, another functionally important adhesion molecule of the DEJZ is collagen VII (COL7A1) (13). It is synthesized and secreted by both epidermal keratinocytes and dermal fibroblasts and undergoes a multistep process of proteolytic maturation and supramolecular assembly to form anchoring fibrils, which secure strong attachment of the epidermis to the underlying dermis (14). Abnormalities of the anchoring fibrils are associated with dystrophic EB, a form of skin fragility in which blisters and wounds heal with scarring (15–17). Its most severe form — generalized recessive dystrophic EB (RDEB), resulting from complete absence of COL7A1 — presents with repeated blistering, wounding, and soft tissue fibrosis leading to disabling deformities (17, 18). A feared complication of RDEB is squamous cell carcinoma, which arises at an early age in trauma-prone skin areas (15, 16). Although clinical observations suggest that wound closure is impaired in RDEB (19–21), no study thus far has addressed the role of COL7A1 in wound healing.

Here, we used 2 different genetic RDEB mouse models to assess the role of COL7A1 in wound healing. In order to validate the find-

Conflict of interest: The authors have declared that no conflict of interest exists.
Citation for this article: *J Clin Invest.* 2013;123(8):3498–3509. doi:10.1172/JCI68127.

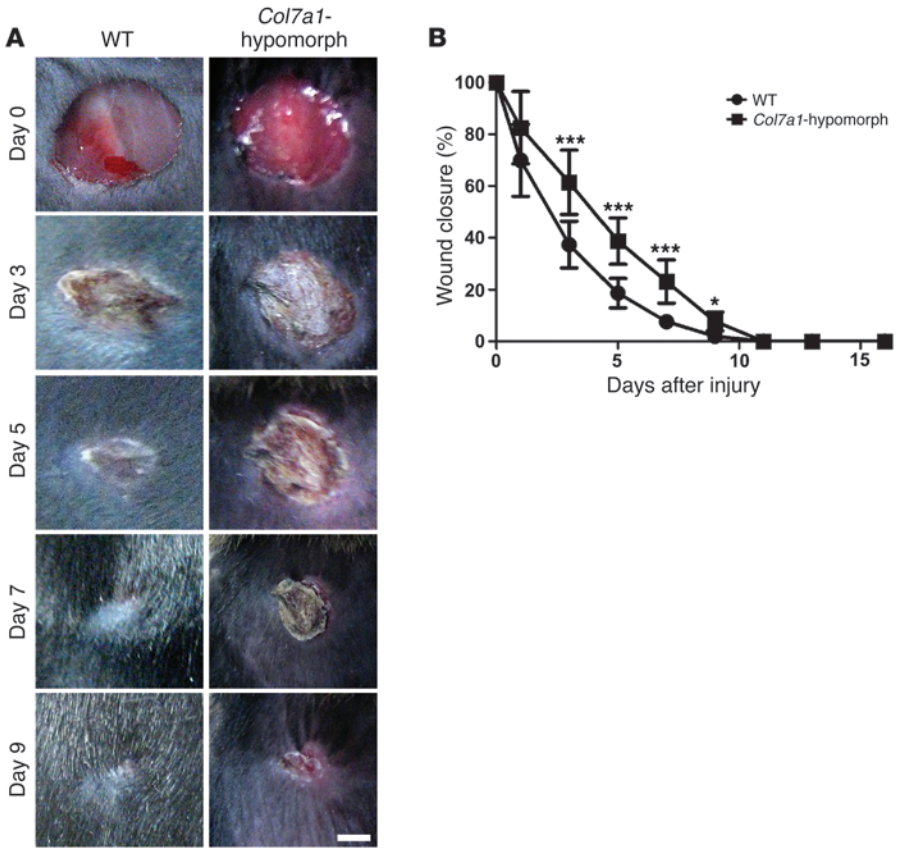

Figure 1
Delayed wound closure in *Col7a1*-hypomorphic mice. (**A**) Closure of 6-mm punch biopsy wounds on the back skin of wild-type and *Col7a1*-hypomorphic mice over time. Scale bar: 2 mm. (**B**) Quantification of the wound area showed significantly delayed gross wound closure between days 3 and 9. n = 14 wounds per group; values represent mean ± SD. $^{*}P < 0.05$; $^{***}P < 0.001$.

ings in the previously described *Col7a1*-hypomorphic mouse (22), an inducible *Col7a1* knockout mouse was generated. The hypomorph has about 10% of physiological levels of wild-type COL7A1, and it replicates all major characteristics of human RDEB (22). The mouse model with tamoxifen-inducible *Col7a1* knockout lacks COL7A1 expression in the healing wounds, but has no chronic disease manifestations in the skin or other organs. Our findings revealed an instrumental role of COL7A1 for both wound re-epithelialization and maturation of the granulation tissue.

Results

Loss of COL7A1 delays re-epithelialization. We sought to delineate the role of COL7A1 in acute skin wound healing, and first found that COL7A1 was present at the provisional DEJZ in early wounds in normal skin (Supplemental Figure 1; supplemental material available online with this article; doi:10.1172/JCI68127DS1). Subsequently, wound healing was analyzed in 2 different COL7A1-deficient mouse models: the *Col7a1*-hypomorphic mouse and a mouse with tamoxifen-inducible *Col7a1* knockout.

During the first 2 days, healing of round, full-thickness wounds showed no differences between wild-type and *Col7a1*-hypomorphic mice. However, between days 3 and 9, *Col7a1*-hypomorphic wounds exhibited significantly delayed closure (Figure 1, A and B). The timing suggested perturbed re-epithelialization, and histomorphological analysis revealed clearly shorter epithelial tongues in *Col7a1*-hypomorphic wounds (Figure 2A). At day 3, the epithelial coverage was 17.8% ± 3.0% in *Col7a1*-hypomorphic wounds versus 30.2% ± 3.8% in wild-type wounds (Figure 2B). At day 7, the epithelial coverage was 87.2% ± 1.5% in COL7A1-deficient skin versus 100% ± 0% in wild-type skin (Figure 2, A and B). The total distance migrated by *Col7a1*-hypomorphic keratinocytes was significantly reduced (Figure 2B), which indicates that the wounds were not larger, but indeed healed slower. Although the *Col7a1*-hypomorphic wounds finally closed, restoration of skin integrity was not adequate, and friction-induced epidermal separation still occurred readily at day 16 (Figure 2C). This is explained at least in part by electron microscopic findings of paucity or absence of anchoring fibrils in *Col7a1*-hypomorphic skin (22). Quantitative assessment of the images revealed significantly reduced width of the dermal-epidermal lamina densa, the layer where COL7A1 is anchored, but no obvious changes of the lamina lucida (Supplemental Figure 2).

Because keratinocytes proliferate to achieve epithelial coverage of larger wounds, it is possible that the difference seen in re-epithelialization was due to increased proliferation. However, this was not the case in COL7A1-deficient wounds, as shown by staining with antibodies against the proliferation marker Ki-67 (Supplemental Figure 3). Thus, loss of COL7A1 delays re-epithelialization by altering keratinocyte migration.

Validation of delayed wound healing in an inducible Col7a1 knockout model. To confirm that the altered wound healing observed in the *Col7a1*-hypomorphic mice was caused by loss of COL7A1, not by other systemic effects, we generated a tamoxifen-inducible *Col7a1* knockout model (Supplemental Figure 4) and subjected the mice to tamoxifen treatment 2 weeks prior to wounding. This led to complete abrogation of COL7A1 expression in both epidermis and dermis in the healing wounds (Supplemental Figure 5A). For these experiments, littermates lacking the Cre box and treated

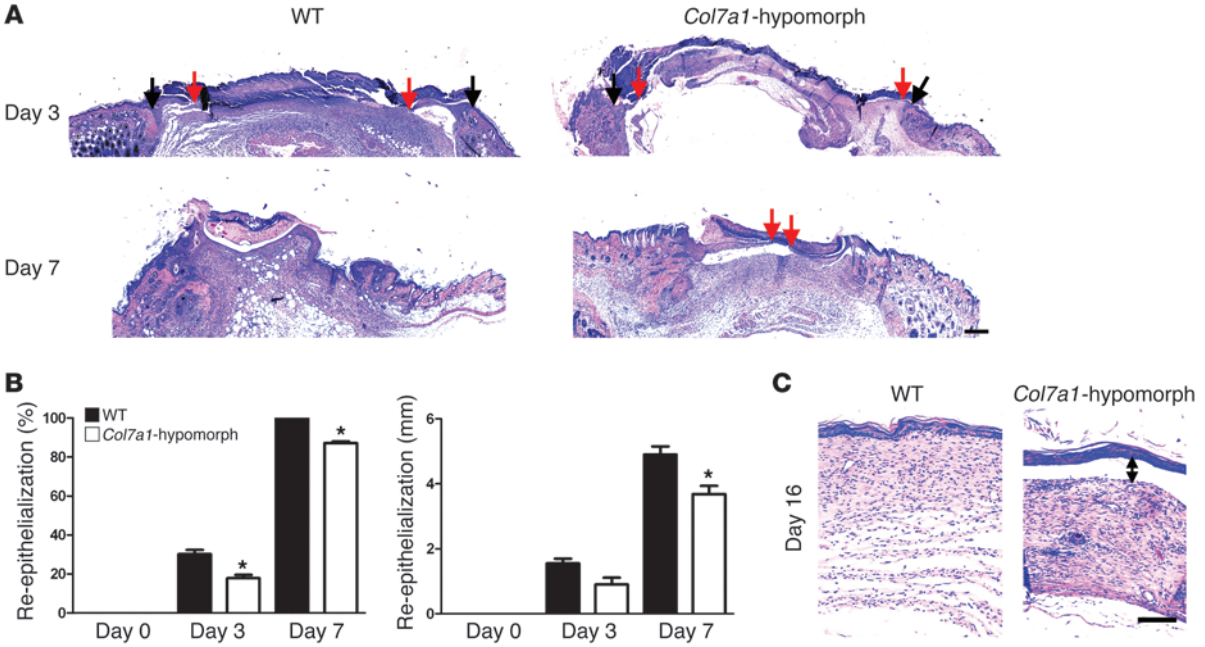

Figure 2

Loss of *Col7a1* delays re-epithelialization. (**A**) H&E staining of wounds in wild-type and *Col7a1*-hypomorphic mice at days 3, 7, and 16. Arrows indicate wound width (black arrows, initial wound border; red arrows, epithelial front). The original wound size was similar, but re-epithelialization was clearly protracted in *Col7a1*-hypomorphic wounds. Scale bar: 500 μm. (**B**) Quantification of percent re-epithelialization (left) and migration distance of the epithelial tongue (right). COL7A1 loss caused a significant delay in re-epithelialization. $n \geq 3$ wounds; values represent mean ± SD. $^*P < 0.05$. (**C**) Wounds after 16 days stained with H&E; note the detached epidermis in the *Col7a1*-hypomorphic wound (double-headed arrow). Note also the changes in the granulation tissue (see also Figure 6 and Supplemental Figure 12). Scale bar: 100 μm.

with tamoxifen served as controls. Mice with tamoxifen-induced *Col7a1* knockout displayed significant retardation of wound closure between days 3 and 9 (Supplemental Figure 5, B and C), and quantification of re-epithelialization showed that induced loss of COL7A1 protracted epithelial coverage. At day 3, the epithelial coverage was 18.2% ± 10.8% in COL7A1-deficient wounds versus 30.1% ± 7.1% in control wounds (Supplemental Figure 5D). Importantly, there was no significant difference in wound healing between the 2 COL7A1-deficient models (Supplemental Figure 6). These observations validated our findings in *Col7a1*-hypomorphic mice and demonstrated that the delay in wound closure was caused by loss of COL7A1 and did not represent a secondary effect.

Altered distribution of laminin-332 and integrin α6β4 in COL7A1-deficient wounds. To clarify how loss of COL7A1 impeded re-epithelialization, we assessed the expression pattern of its major ligand, laminin-332, in 7-day-old wounds. Absence of COL7A1 altered laminin-332 deposition, as shown by an irregular, broad, and patchy laminin-332 immunofluorescence signal at the DEJZ in *Col7a1*-hypomorphic skin, in contrast to the distinct linear staining in wild-type wounds (Figure 3A). The alterations were most evident in areas that had just undergone, or were about to undergo, fusion of the epidermal tongues (Figure 3A).

Expression of integrin α3β1, the principal laminin-332 receptor on migrating keratinocytes, was unchanged (Figure 3A and data not shown). However, the other major laminin-binding integrin on keratinocytes, integrin α6β4, displayed a strikingly broad and suprabasal expression pattern in *Col7a1*-hypomorphic mice (Figure 3A). Altered distribution of laminin-332 and integrin α6β4 was also observed in areas of active keratinocyte migration (Figure 3, B and C), and suprabasal integrin α6β4 expression persisted after completion of re-epithelialization (Figure 3C). Wounds in the inducible *Col7a1* knockout mouse corroborated these findings (Supplemental Figure 7), validating the causal link between COL7A1 deficiency and aberrant expression of laminin-332 and integrin α6β4. Taken together, these results indicate that loss of COL7A1 affects the organization of laminin-332 at the DEJZ, which in turn perturbs the spatially restricted expression of integrin α6β4 in regenerating epidermis.

Loss of COL7A1 perturbs the laminin-332/integrin α6β4 signaling axis. To assess the consequences for keratinocyte signaling, we investigated 2 downstream components of the laminin-332/integrin α6β4 signaling axis, JNK and STAT3. Upon activation of integrin α6β4, these factors become phosphorylated in the cytosol and translocate to the nucleus (23, 24). Accordingly, in wild-type wounds, nuclear expression of JNK and STAT3 was observed in basal cells of the leading wound edge, but in *Col7a1*-hypomorphic wounds, suprabasal keratinocytes at the wound edge displayed significantly increased nuclear STAT3 and JNK (Figure 4A). These changes persisted in more mature, fully re-epithelialized wounds (Figure 4B).

In vitro, keratinocytes derived from *Col7a1*-hypomorphic mice closed scratch wounds slightly, but significantly slower than wild-type keratinocytes (Figure 5A). The difference in migration became evident after 8 hours, when sufficient time had lapsed for the cells to synthesize and deposit COL7A1. Western blot analysis revealed an approximately 2-fold increase of the integrin β4 subunit in *Col7a1*-hypomorphic keratinocytes (Figure 5B), and quantification of immunofluorescence staining of integrin β4 in basal keratino-

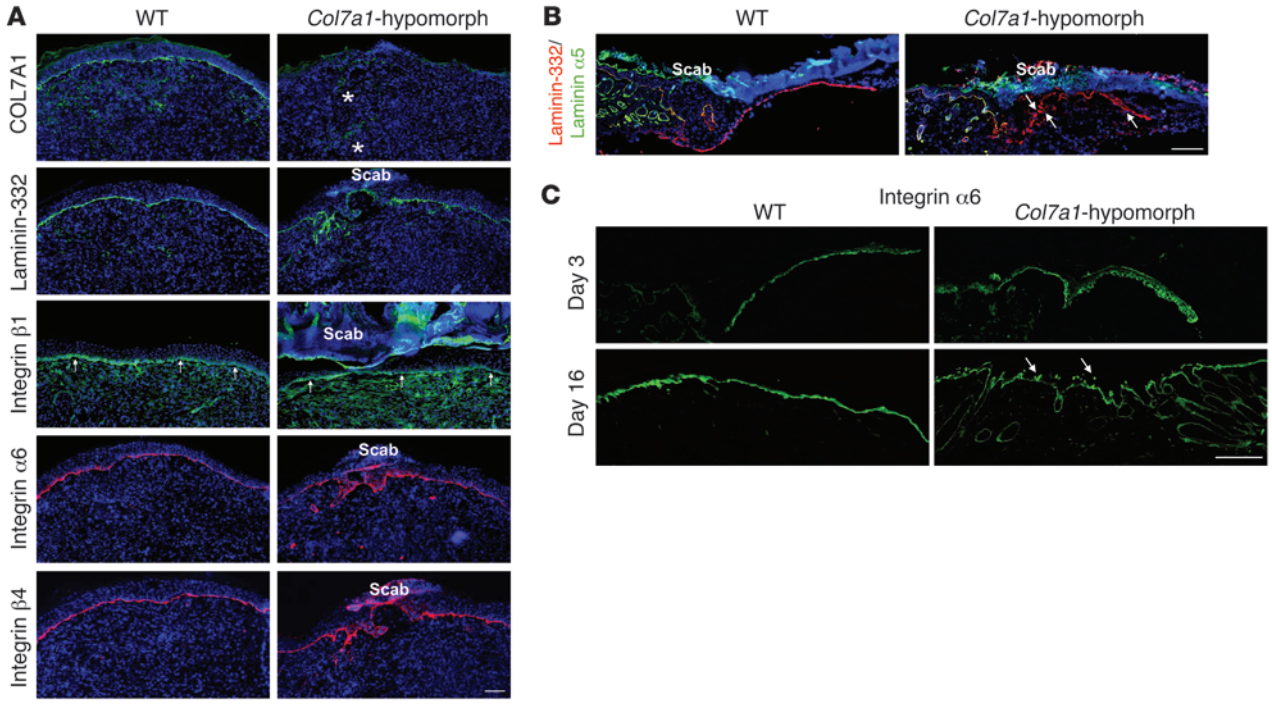

Figure 3

Loss of COL7A1 alters laminin-332 deposition and integrin α6β4 distribution in healing epidermis. (**A**) 7-day wounds stained for laminin-332 and its integrin receptors. Laminin-332 deposition and integrin α6β4 distribution was altered in *Col7a1*-hypomorphic wounds. Asterisks show autofluorescence from red blood cells trapped in capillaries; arrows point to integrin β1 at the DEJZ. Scale bar: 100 μm. (**B**) Epidermal tongue in 3-day wounds stained for laminin-332 (red) and the laminin α5 chain (green). Laminin-332 deposition was irregular and patchy in *Col7a1*-hypomorphic wounds (arrows), in contrast to the distinct linear signal of the laminin α5 chain. Scale bar: 50 μm. (**C**) 3- and 16-day-old wounds stained for integrin α6. Arrows indicate the patchy suprabasal integrin α6 expression in 16-day-old *Col7a1*-hypomorpic wounds. Scale bar: 50 μm.

cytes in 7-day-old wounds supported this observation (Supplemental Figure 8). Furthermore, the downstream targets of integrin α6β4, JNK2 and AKT, were significantly more phosphorylated in *Col7a1*-hypomorphic keratinocytes (Figure 5, C and D), indicative of perturbed integrin α6β4 signaling.

Keratinocytes from inducible *Col7a1* knockout mice were divided into 2 pools: in the first pool, *Col7a1* knockout was induced by 4-OH tamoxifen treatment, while the second pool received only DMSO vehicle. After verification of efficient *Col7a1* knockout (Supplemental Figure 4, B and C), cells were harvested for analysis of integrin α6β4 signaling. Forced COL7A1 loss resulted in activation of JNK2 and AKT (Figure 5E and Supplemental Figure 9), corroborating our findings in *Col7a1*-hypomorphic keratinocytes that COL7A1 regulates laminin-332/integrin α6β4 signaling.

Although 2-dimensional cell culture does not allow assembly of complex structures such as the DEJZ, there are indications that COL7A1 is important for laminin-332 organization in this system (25). In the present study, loss of COL7A1 in *Col7a1*-hypomorphic keratinocytes and in conditional keratinocytes after 4-OH tamoxifen treatment resulted in a remarkable pericellular accumulation of laminin-332 (Figure 5F), although synthesis of laminin-332 was not increased (Figure 5E and Supplemental Figure 10). Interestingly, the aberrant laminin-332 deposition and activation of the laminin-332/integrin α6β4 signaling axis in COL7A1-deficient keratinocytes could be normalized by addition of recombinant COL7A1 (Supplemental Figure 11). Thus, the data clearly demonstrated that loss of COL7A1 leads to aberrant laminin-332 organization by epidermal keratinocytes and consequently modulates integrin α6β4 signaling. This is likely the underlying cause of the altered migration of COL7A1-deficient keratinocytes in vitro and in vivo.

COL7A1 influences dermal fibroblast functions during wound closure. Since COL7A1 is synthesized by both keratinocytes and dermal fibroblasts, it is plausible that its loss would affect granulation tissue formation in injured dermis. At day 7 after wounding, it was apparent that this was the case: *Col7a1*-hypomorphic mice exhibited both abnormal localization of myofibroblasts and prolonged presence of inflammatory cells (Figure 6), indicative of delayed granulation tissue and wound maturation. In wild-type wounds, α-SMA–positive myofibroblasts were localized in the center of the granulation tissue, whereas in *Col7a1*-hypomorphic wounds, they remained at the wound edges 2 days longer (Figure 6A). Quantification of total CD11b cell count, α-SMA–positive area, and granulation tissue thickness during wound healing clearly supported the observation of protracted dermal healing (Supplemental Figure 12, A–C). Similarly, in the inducible mouse model, myofibroblast maturation in the granulation tissue was delayed; at day 7 after wounding, the α-SMA–positive myofibroblasts were preferentially present at the wound rim, not condensed toward the middle, as seen in wild-type wounds (Supplemental Figure 5E).

The next question was whether COL7A1 exerts a direct, keratinocyte-independent effect on fibroblasts during wound healing. Interestingly, the granulation tissue in wild-type wounds contained COL7A1 deposits, which were absent in *Col7a1*-hypo-

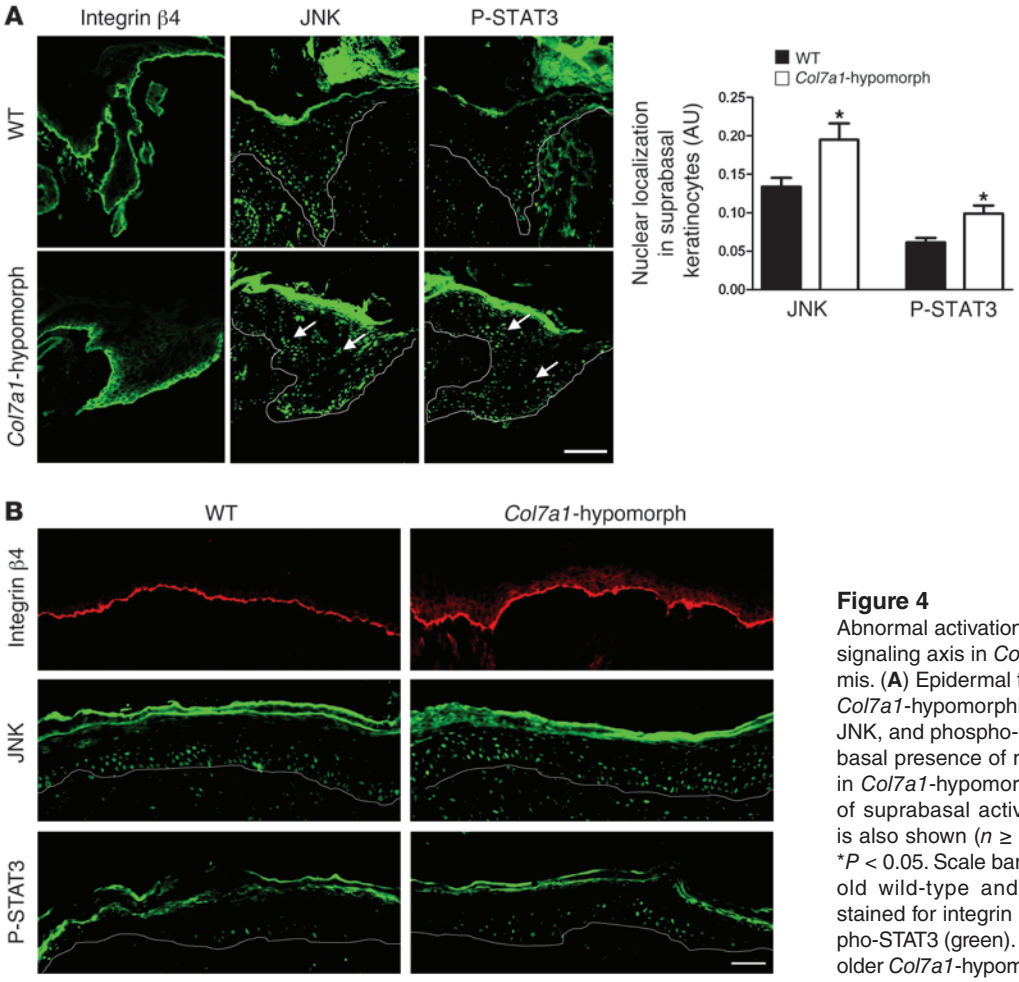

Figure 4
Abnormal activation of the laminin-332/integrin α6β4 signaling axis in *Col7a1*-hypomorphic wound epidermis. (**A**) Epidermal tongue of 3-day-old wild-type and *Col7a1*-hypomorphic wounds stained for integrin β4, JNK, and phospho-STAT3. Note the abundant suprabasal presence of nuclear JNK and phospho-STAT3 in *Col7a1*-hypomorphic wounds (arrows), indicative of suprabasal activation. Quantification of staining is also shown ($n \geq 3$; values represent mean ± SD). $^*P < 0.05$. Scale bar: 50 μm. (**B**) Middle area of 7-day-old wild-type and *Col7a1*-hypomorphic wounds stained for integrin β4 (red), JNK (green), and phospho-STAT3 (green). Suprabasal activation persisted in older *Col7a1*-hypomorphic wounds. Scale bar: 50 μm.

morphic mice (Figure 7A). Since fibroblast migration is critical for formation of granulation tissue, fibroblasts isolated from wild-type and *Col7a1*-hypomorphic skin were subjected to wound closure scratch assays in vitro. Within 24 hours, wild-type fibroblasts closed the scratch wounds completely, but *Col7a1*-hypomorphic cells did that only to about 80% (Figure 7B), arguing for a supportive role of COL7A1 in fibroblast migration during wound healing.

In order to assess the signaling mechanisms leading to delayed granulation tissue formation, we serum-stimulated starved dermal fibroblasts, an experimental setup that has previously been shown to replicate gene expression changes during wound healing (26). Notable changes in *Tgfb1* and *Fgf2* expression were observed in *Col7a1*-hypomorphic fibroblasts: *Tgfb1* expression was increased 4.7-fold, and *Fgf2* expression was reduced 6.3-fold (Figure 7C). Importantly, *Tgfb1* expression was not altered in COL7A1-deficient keratinocytes (Supplemental Figure 13). Immunofluorescence staining demonstrated that TGF-β1 protein was increased in the granulation tissue in healing wounds in *Col7a1*-hypomorphic mice compared with wild-type controls (data not shown), and TGF-β signaling was activated, as seen by increased SMAD2 phosphorylation (Figure 7D). Since TGF-β signaling via SMADs potently stimulates collagen I production (27), we also investigated collagen I deposition in the granulation tissue. Interestingly, the granulation tissue of 7-day-old *Col7a1*-hypomorphic wounds contained significantly elevated levels of collagen I (Supplemental Figure 12, D and E). These data clearly indicate that loss of COL7A1 from the healing dermis causes abnormal TGF-β activation.

To test the possibility that COL7A1 directly influences fibroblast gene expression, *Col7a1*-hypomorphic fibroblasts were cultured on plates coated with collagen I, alone or in combination with recombinant COL7A1. In this system, addition of exogenous COL7A1 reverted the altered expression of *Tgfb1* and *Fgf2* (Figure 7E). Thus, we conclude that COL7A1 within the granulation tissue has a specific function in supporting migration of fibroblasts and regulating their cytokine production during wound healing.

Human RDEB wounds display altered laminin-332 deposition and integrin α6β4 expression. To validate the above findings in a human setting, we analyzed fresh surgical wounds, wound margins of chronic wounds, and wounds from RDEB patients. We focused on altered epidermal expression of laminin-332 and integrin α6β4, since healing through contraction plays a lesser role in human skin than in rodent skin (1), and since the granulation tissue phenotype is transient and not targetable in spontaneous wounds of patients. Fresh wounds showed linear deposition of laminin-332, exhibited basal expression of integrin α6, and were positive for COL7A1 at the healing DEJZ (Figure 8A). In contrast, COL7A1-negative RDEB wounds displayed disorganized laminin-332 deposition, with dense deposits alternating with laminin-332–sparse regions, and disor-

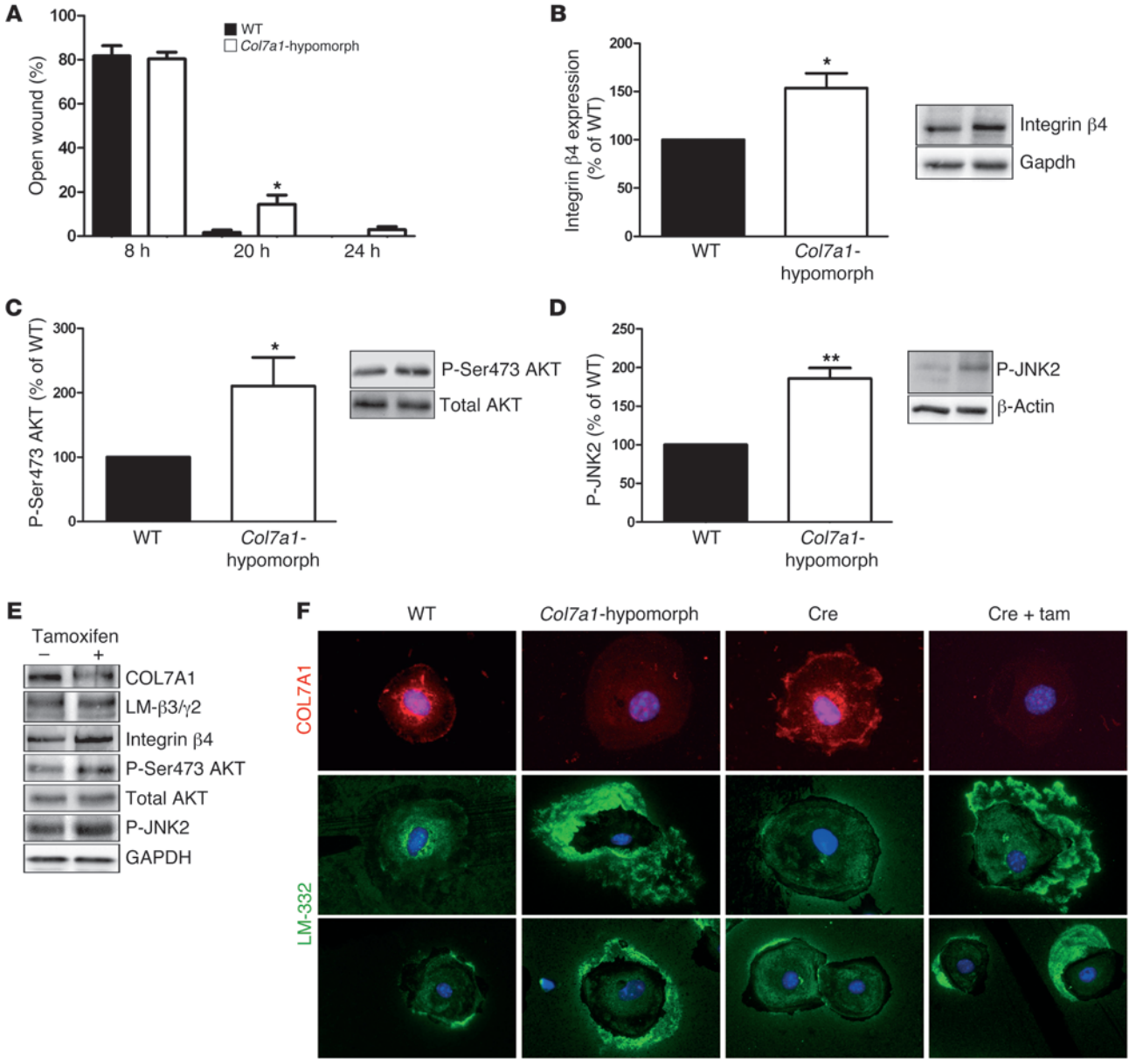

Figure 5

Mechanisms of delayed wound closure in *Col7a1*-hypomorphic keratinocytes. (**A**) In vitro assays, wound closure by keratinocytes was assessed at 8, 20, and 24 hours. At 20 and 24 hours, *Col7a1*-hypomorphic keratinocytes closed wounds at a reduced rate. $n = 6$; values represent mean ± SEM. $^*P < 0.05$. (**B**–**D**) Western blotting of wild-type and *Col7a1*-hypomorphic keratinocyte protein lysates revealed increased expression of integrin β4 subunit (**B**) and increased phosphorylation of Ser473 AKT (**C**) and JNK2 (**D**) in cultured *Col7a1*-hypomorphic keratinocytes. Densitometric quantification of keratinocyte isolations is also shown. $n \geq 3$; values represent mean ± SD. $^*P < 0.05$; $^{**}P < 0.01$. (**E**) Western blots on cell lysates from tamoxifen-induced *Col7a1* knockout mouse keratinocytes. Keratinocytes from the same isolation were divided into 2 pools: one was treated with 4-OH tamoxifen to induce *Col7a1* knockout, the other received only DMSO and served as control. The changes in *Col7a1*-hypomorphic keratinocytes were replicated in keratinocytes after forced COL7A1 loss. Loss of COL7A1 did not affect expression of laminin-332 (LM-β3/γ2; representing the laminin β3 and γ2 chains of laminin-332), but increased expression of integrin β4 and phosphorylation of Ser473 AKT and JNK2. Total AKT and GAPDH were used to ensure equal loading. (**F**) Altered Laminin-332 organization in *Col7a1*-hypomorphic keratinocytes. Primary keratinocytes of the indicated genotypes and treatments were cultured for 24 hours in the presence of ascorbate and stained for COL7A1 (red) and laminin-332 (green). Original magnification, ×400. Tam, tamoxifen.

ganized suprabasal expression of integrin α6 (Figure 8A). Chronic wounds displayed similarities to RDEB wounds, with disorganized laminin-332 and integrin α6; importantly, these wounds also showed reduction or loss in COL7A1 under the healing epidermis.

To investigate whether human wounds also show activation of downstream targets of laminin-332/integrin α6β4 signaling, in agreement with our findings in mice, we analyzed them for JNK and STAT3 phosphorylation. In fresh wounds, similar to wild-

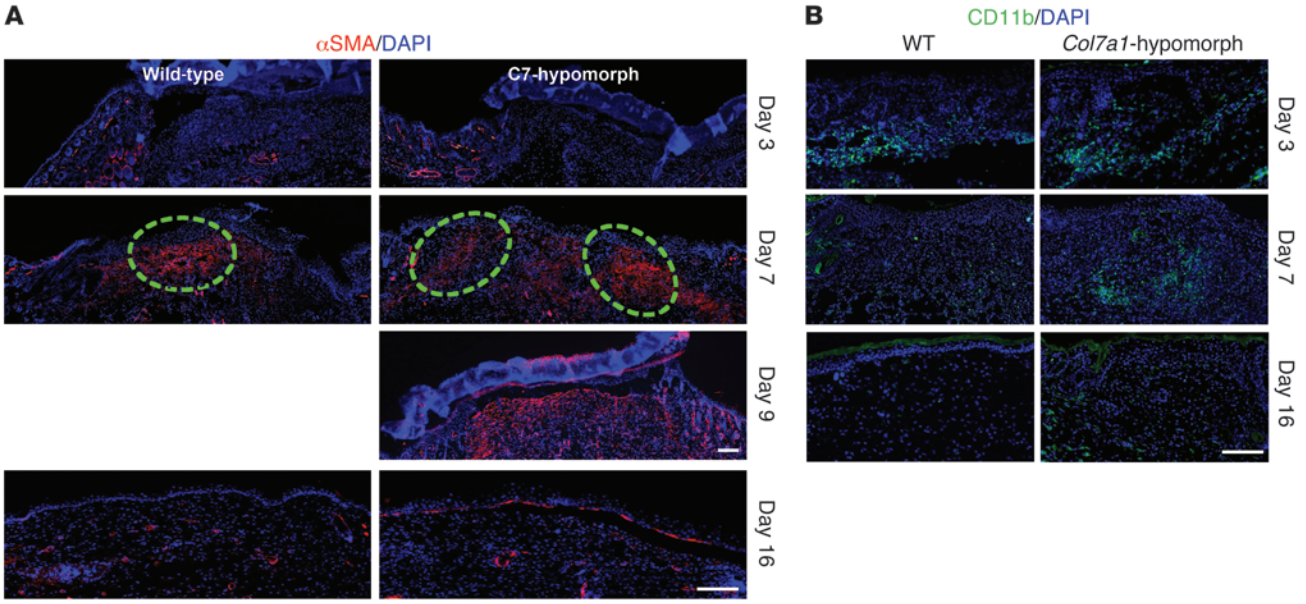

Figure 6
Granulation tissue maturation and clearance of inflammatory cells are delayed in *Col7a1*-hypomorphic wounds. (**A**) α-SMA staining (red) showed few myofibroblasts at the wound edge at day 3 in both wild-type and *Col7a1*-hypomorphic mice. At day 7, myofibroblasts were abundant in the middle of the wild-type wound, but remained in the periphery of the *Col7a1*-hypomorphic wound. Dashed outlines denote the dense myofibroblast regions. Myofibroblast organization in the day 9 *Col7a1*-hypomorphic wound was similar to that of 7-day wild-type wounds, with myofibroblasts localized in the upper central part of the granulation tissue. At day 16 after wounding, most myofibroblasts had disappeared in both mice. Nuclei were stained with DAPI (blue). Scale bars: 100 μm. (**B**) CD11b staining (green) revealed protracted clearance of inflammatory cells in *Col7a1*-hypomophic wounds. At day 3, inflammatory cells were at the wound edge in both wild-type and *Col7a1*-hypomorphic mice. At day 7, inflammatory cells were mainly seen in the middle of the wound in both mice. At day 16, CD11b-positive cells were cleared from the wound area in wild-type mice, but not in *Col7a1*-hypomorphic mice. Nuclei were stained with DAPI (blue). Scale bar: 100 μm. See Supplemental Figure 12 for quantification of granulation tissue changes.

type mouse wounds, JNK and STAT3 phosphorylation was mainly restricted to basal keratinocytes in the healing epidermis (Figure 8B). However, both RDEB and chronic wounds showed strong and abundant suprabasal JNK and STAT3 activation (Figure 8B). These findings in human wounds mirrored the situation in our RDEB mouse models and validated the delayed re-epithelialization in human RDEB skin. In addition, they implicate COL7A1 as an important modulator of healing of other chronic wounds.

Discussion

Here, we demonstrated that COL7A1 is not only vital for maintaining skin integrity, but is also a critical player in skin wound closure. Loss of COL7A1 compromises wound repair by 2 separate, yet interconnected events: delayed re-epithelialization by epidermal keratinocytes and perturbed granulation tissue maturation by dermal fibroblasts.

Previous in vitro models have delivered contradictory findings relating to the role of COL7A1 in keratinocyte migration. COL7A1 has been found to directly support keratinocyte migration (28), but another model using epithelial cancer cell lines suggested an inhibitory role (29). In the present study, abrogation of COL7A1 significantly slowed scratch wound closure by primary keratinocytes (Figure 5A), which strongly indicates that COL7A1 supports keratinocyte migration.

In vivo, in a COL7A1-deficient environment, wound keratinocytes altered their integrin α6β4 expression and deposition of laminin-332 into the provisional extracellular matrix laid out under the migrating cell front. Both phenomena contributed to protracted re-epithelialization of COL7A1-deficient skin wounds, but aberrant laminin-332 organization is likely to be the main cause. Laminin-332 is commonly believed to be a promoter of epithelialization during wound healing (30–32), despite some controversy in the literature (33, 34). Here, we found that irregular deposition of laminin-332 was associated with delayed migration of the epidermal tongues in the absence of COL7A1 in vivo, which indicates that not the sheer presence of laminin-332, but its assembly and deposition, play a functional role. This is congruent with a recent observation that the polymerization status of laminin-332 is important for determining its effect on keratinocytes (35). Purified nonpolymerized laminin-332 readily promoted keratinocyte migration, whereas polymerized laminin-332 matrices inhibited migration by supporting integrin α3β1 adhesion and integrin α6β4–dependent hemidesmosome formation (34).

Abnormal laminin-332 organization in COL7A1-deficient wounds can be accounted for by 2 events. First, COL7A1 — with its strong affinity for laminin-332 — is important for establishing correct laminin-332 architecture at the DEJZ (25), which determines interactions with extracellular ligands and cell surface receptors and, ultimately, cell-signaling activities. Second, the laminin-332 receptor integrin α6β4 is important for regulating laminin-332 deposition in a process that involves Rac-1 activation (9). Keratinocytes lacking the integrin β4 subunit lay out laminin-332 in an abnormal circular fashion, which affects cell movement in vitro (9). Since COL7A1-deficient wound epidermis displays increased

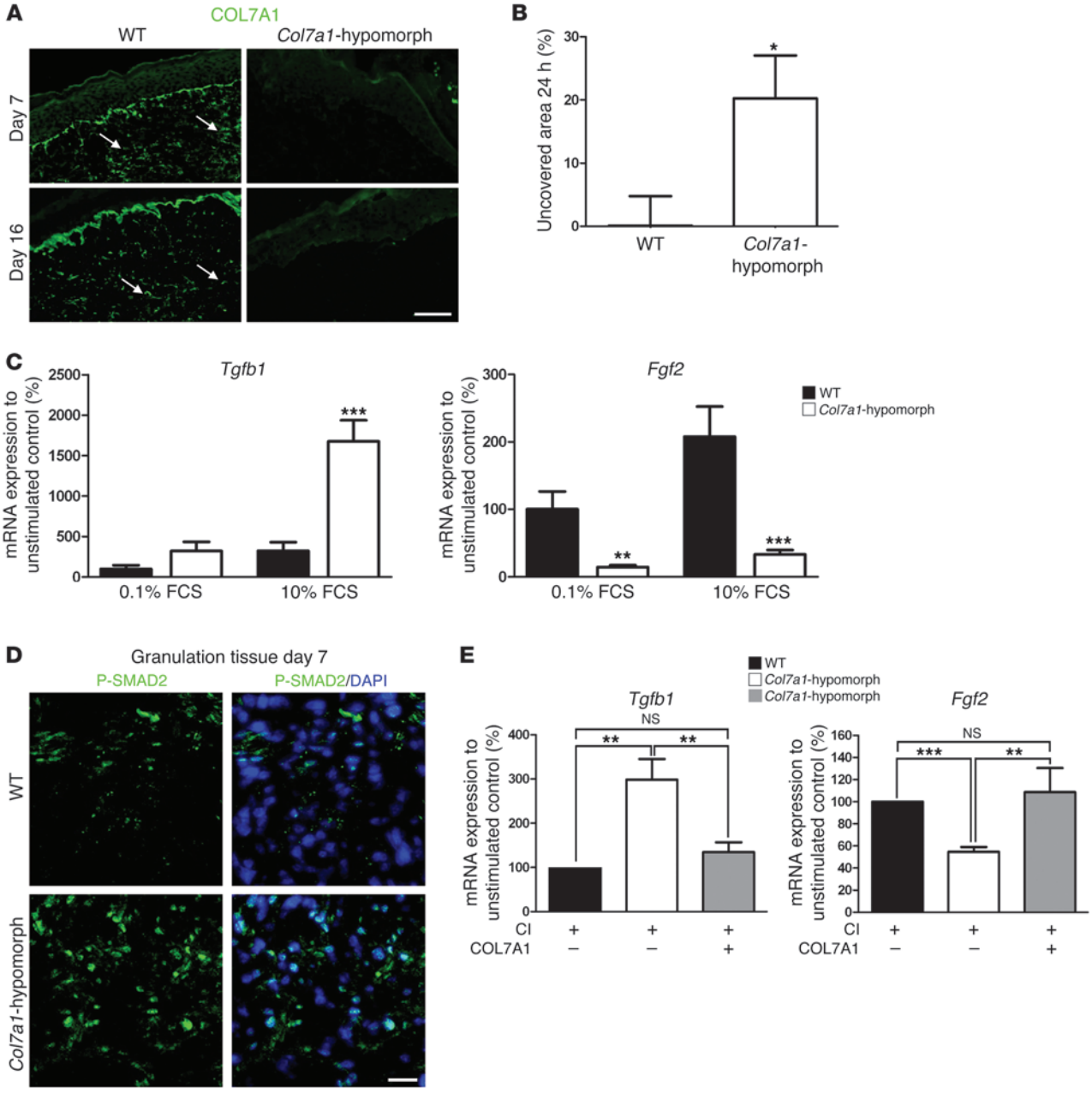

Figure 7

COL7A1 affects dermal fibroblasts during wound healing. (**A**) Granulation tissue in 7- and 16-day wounds in wild-type and *Col7a1*-hypomorphic mice stained for COL7A1 (green). Note the presence of COL7A1 aggregates (arrows) within the healing dermis in wild-type mice. Scale bar: 50 μm. (**B**) In vitro scratch wound assay. *Col7a1*-hypomorphic fibroblasts closed the scratch wound significantly slower than did wild-type cells. $n = 7$. (**C**) Serum-response assay, which replicates fibroblast signaling events during wound healing (26). Dermal fibroblasts were starved in 0.1% FCS for 48 hours, stimulated with 10% serum for 5 hours, and analyzed for gene expression. *Tgfb1* and *Fgf2* mRNA expression were normalized to *Gapdh* and a nonstimulated control. Serum stimulation substantially increased *Tgfb1* mRNA expression, but reduced *Fgf2* expression, in *Col7a1*-hypomorphic compared with wild-type fibroblasts. $n = 5$. (**D**) P-SMAD2 staining (green) of granulation tissue in day-7 wounds confirmed increased activation of TGF-β1 signaling in the *Col7a1*-hypomorphic wound. Nuclei were visualized with DAPI (blue). Scale bar: 20 μm. (**E**) Supplementation of recombinant COL7A1 to *Col7a1*-hypomorphic fibroblasts normalized *Tgfb1* and *Fgf2* expression. Dermal fibroblasts were grown on 1.5 μg collagen I (CI), with or without 1.5 μg/well recombinant COL7A1, until they reached confluence, then serum-starved for 48 hours and stimulated with 10% FCS for 5 hours. mRNA expression was analyzed as in **C**. $n \geq 4$. All values represent mean ± SEM. $^*P < 0.05$, $^{**}P < 0.01$, $^{***}P < 0.001$.

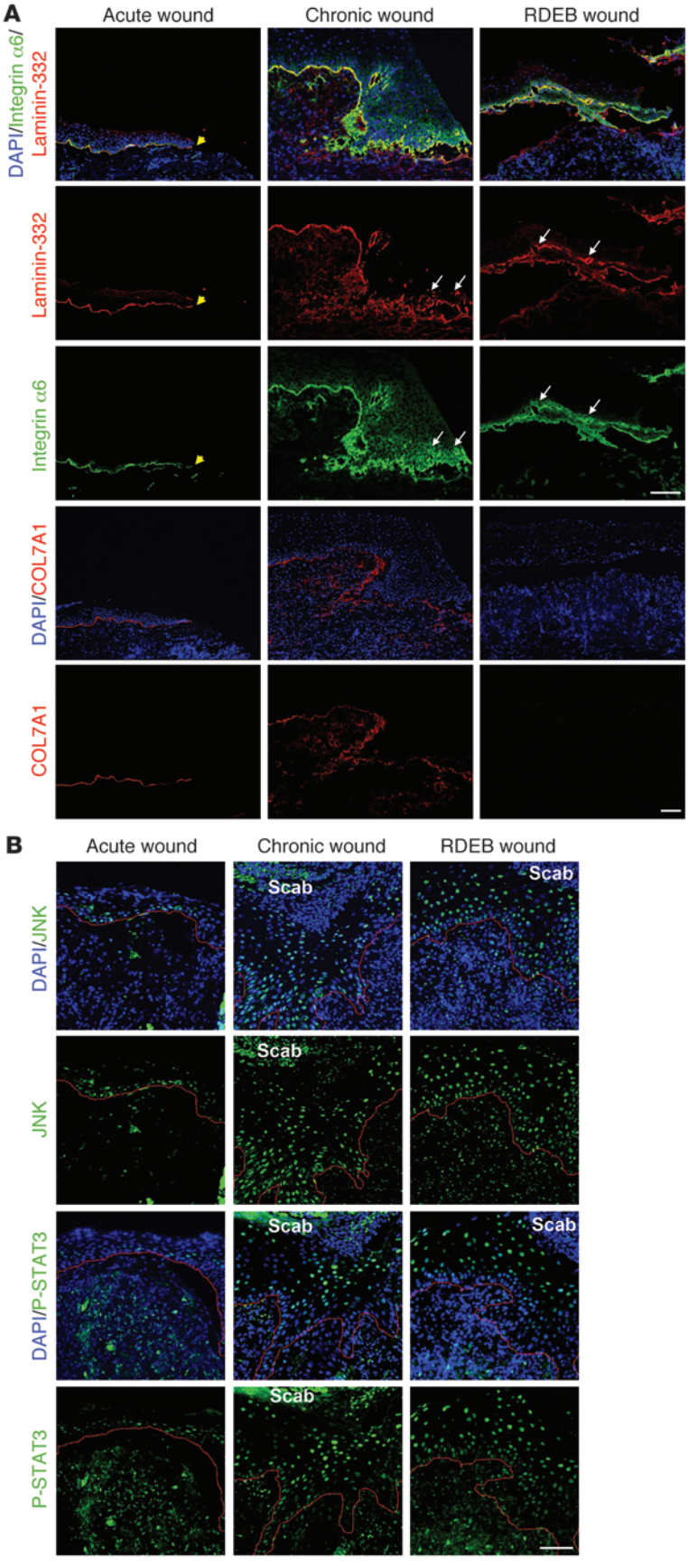

Figure 8
Human RDEB and other chronic wounds display similar molecular alterations. Wound biopsies were obtained from fresh wounds 3 days after primary excision (Acute wound), from the wound margins of nonhealing chronic venous ulcers, and from wounds of RDEB patients. (**A**) Wounds were stained for laminin-332 (red) and integrin α6 (green) or for COL7A1 (red). Yellow arrowheads denote the end of the epithelial front in the acute wound. For chronic and RDEB wounds, the epithelial front in the wound margin is shown. Acute wounds showed linear deposition of laminin-332 and regular, primarily basal, expression of integrin α6, whereas in chronic and RDEB wounds, laminin-332 deposition was irregular and integrin α6 expression suprabasal (white arrows). Importantly, in acute wounds, COL7A1 was distinctly present under the healing epidermis, whereas it was irregular and drastically reduced in chronic wounds. Nuclei were visualized with DAPI (blue). Scale bar: 50 μm. (**B**) Epidermal tongues in wound margins stained for phospho-JNK (green) or phospho-STAT3 (green). Nuclei were counterstained with DAPI (blue). Red lines denote the epidermal-dermal interface. In acute wounds, phospho-JNK and phospho-STAT3 staining was weak and mainly seen in basal keratinocytes, whereas both chronic and RDEB wounds showed strong phospho-JNK and phospho-STAT3 staining in suprabasal keratinocytes. Scale bar: 50 μm.

and broadened integrin α6β4 distribution, it is conceivable that this contributes to the altered laminin-332 organization.

Depending on the biological context, integrin α6β4 can be both a driver and an inhibitor of cell migration, at least in vitro (24, 36, 37). Interestingly, in in vitro migration assays, we observed subtle differences in migration behavior between wild-type and COL7A1-deficient keratinocytes. In wild-type wounds, single cells were observed migrating ahead of the collective front. This was not found in *Col7a1*-hypomorphic wounds, where strict collective migration was seen (data not shown). In light of these observations, it is interesting that integrin α6β4 has been suggested to delay haptotaxis by activating E-cadherin, leading to tighter cell-cell contacts (38). Our observations of altered migration behavior in integrin α6β4–overexpressing COL7A1-deficient keratinocytes support these studies. However, caution must be taken since the in vivo situation is much more complex; it is possible that in COL7A1-deficient wounds, aberrant epidermal integrin α6β4 expression does not primarily influence keratinocyte migration, but has other consequences for RDEB skin, for example, priming it for malignant transformation (39).

In the dermal compartment, loss of COL7A1 led to protracted maturation of granulation tissue, including lingering maturation of myofibroblasts and slower clearance of inflammatory cells. In vitro, *Col7a1*-hypomorphic fibroblasts closed scratch wounds significantly slower (Figure 7B). These observations are in line with the prior demonstration that COL7A1 supports adhesion of dermal fibroblasts through the col-

lagen receptor integrin α2β1 (40, 41). Since integrin α2β1 also drives cell migration on many other collagens (42), it is likely to sustain migration also on COL7A1. Therefore, we conclude that the delayed fibroblast migration and delayed granulation tissue formation in the *Col7a1*-hypomorphic mouse are direct consequences of COL7A1 loss.

The altered cytokine profiles in *Col7a1*-hypomorphic fibroblasts were reverted by exogenous COL7A1 (Figure 7E), which indicates that COL7A1 modulates signaling in fibroblasts, in line with a recent study using gene expression arrays (43). Most importantly, loss of COL7A1 led to increased production of TGF-β1, which stimulates synthesis of extracellular matrix and scarring in RDEB (43–45). TGF-β signaling and tissue stiffness drive myofibroblast differentiation (46–48). The delay in myofibroblast maturation in COL7A1-deficient wounds emphasizes the importance of COL7A1 for fibroblast migration, but also shows that lack of COL7A1 results first in a softer provisional dermal matrix that does not support TGF-β activation and myofibroblast development (46), and later, as a consequence of repeated wounding in RDEB, in TGF-β1–mediated stimulation of extracellular matrix synthesis and soft tissue fibrosis (49).

The persistence of macrophages and neutrophils in the healing COL7A1-deficient dermis can also be explained by continuously high levels of TGF-β1, which attracts neutrophils, macrophages, and fibroblasts (4). Its continuous presence thus hampers resolution of inflammation.

A common downstream connector for the effects on wound keratinocytes and fibroblasts upon loss of COL7A1 is the secreted actin-remodeling protein Flightless I (Flii). Flii is upregulated in wounds (50) and in *Col7a1*-hypomorphic skin (51), and its overexpression slows healing of skin wounds by altering both re-epithelialization and wound contraction (50). In addition, Flii overexpression stimulates TGF-β1 production (51). However, it is important to note that the primary cause of the reduced wound healing of COL7A1-deficient skin lies in loss of COL7A1 and perturbed signaling by the microenvironment; aberrant Flii expression is one consequence of the faulty matrix.

In conclusion, COL7A1 is pivotal for both epidermal re-epithelialization and dermal granulation tissue development during closure of skin wounds. Loss of COL7A1 negatively affects both processes and results in distinct molecular changes that explain the immediate pathology of RDEB wounds as well as the long-term complications of the disorder and other chronic wounds.

Methods

Antibodies and proteins. The following antibodies were used: mouse anti-GAPDH (Millipore), rabbit anti–COL7A1 (Millipore), mouse anti–β-actin (Sigma-Aldrich), rabbit anti-tubulin (Abcam), rat anti–integrin α6 (GoH3) (Progen), rat anti–integrin β1 (BD Biosciences), rat anti–integrin β4 (BD Biosciences), rabbit anti–integrin β4 (Santa Cruz Biotechnology), mouse anti–active JNK1 and JNK2, rabbit anti-JNK (Abcam), rabbit anti–phospho–Tyr705 STAT3 (Cell Signaling Technology), mouse anti-AKT (Santa Cruz Biotechnology), rabbit anti–phospho–Ser473 AKT (Cell Signaling Technology), rat anti–Ki-67 (Dako), Cy3-conjugated mouse anti–α-SMA (Sigma-Aldrich), rat anti-CD11b (BD Biosciences), rabbit anti-mouse collagen I (Acris), rabbit anti–laminin-332 (gift from K. Yancey, University of Texas Southwestern, Dallas, Texas, USA), rabbit anti–pan-laminin (Progen), and rat anti–laminin α5 (gift from L. Sorokin, Muenster University, Muenster, Germany). Secondary antibodies were Alexa Fluor 488– and Alexa Fluor 594–conjugated goat anti-rabbit IgG (Invitrogen), Alexa Fluor 488– and Alexa Fluor 568–conjugated goat anti-rat IgG (Invitrogen), HRP-conjugated goat anti-mouse and anti-rabbit (Jackson Immuno Research Laboratories Inc.). Rat tail collagen I was obtained from BD Biosciences, and human recombinant COL7A1 was produced and purified using an inserted FLAG tag at the N-terminus, as previously described (52).

Transgenic mice. Mice were housed in the pathogen-free facility at the University of Freiburg and given food and water ad libitum; in addition, *Col7a1*-hypomorphic mice were provided with a soft food diet for extra support, as previously described (22). See Supplemental Methods for details.

Electron microscopy. Electron microscopic analysis of the skin has been described previously (22). Briefly, adult wild-type or *Col7a1*-hypomorphic littermates were shaved, after which skin was harvested, cut out, and fixed in 4% paraformaldehyde and 2% glutaraldehyde. After fixation, the skin was washed in 0.1 M cacodylate buffer, followed by incubation in 1% osmium tetroxide solution. Samples were dehydrated in ethanol and propylene oxide and embedded in epoxide resin. Sections were cut and mounted on microscopy grids and stained with 5% uranyl acetate and Reynold's solution. Quantification of lamina lucida and densa of randomly selected areas was performed using Image J software (NIH).

Assessment of wound healing. The mice used for the wound-healing studies were 4- to 6-week-old *Col7a1*-hypomorphic mice and their wild-type littermates. The backs of the mice were shaved and sterilized, and wounding was performed under isoflurane anaesthesia. 2 full-thickness wounds per mouse were created by punching a 6-mm biopsy tool (Pfm medical) through a skin fold on the mid-back; the wounds were thus positioned at a place with limited accessibility for hindpaws, forepaws, and mouth to avoid secondary traumatization of the healing wounds by scratching or biting. Use of protective wound dressings was not possible, since daily dressing removal and changing damages the fragile skin of the *Col7a1*-deficient mice. Instead, mice were kept in individual cages after wounding and monitored every day for rewounding. Wounds were photographed with a Canon power shot S3IS camera (Canon) directly after infliction, the following day, and then every other day until sacrifice. Photos were captured in a standardized way, with sticky rulers used for reference. Gross wound closure was quantified by Image J (NIH), and wound healing was expressed as the percentage of the original wound area that had healed, calculated as $(1 - [\text{wound area day } x/\text{wound area day } 0]) \times 100$. After sacrifice, the wound tissue was carefully dissected and fixed in formalin for histopathological analysis or embedded in Tissue-Tek OCT compound (Sakura) and snap frozen for immunofluorescence analysis. Re-epithelialization was determined by H&E staining of serial sections from the middle of the wounds; images were acquired using an Axiocam MRm camera attached to a Zeiss Axio Imager A1 microscope (Carl Zeiss). Percent re-epithelialization and migration distance of the epithelial tongue were quantified with Image J. Elastica van Gieson staining was performed as described previously (22).

Isolation and culture of murine keratinocytes and fibroblasts. Keratinocytes and fibroblasts were isolated from newborn mice and cultured as previously described (53, 54).

For induction of *Col7a1* knockout, keratinocytes and fibroblasts were treated with 1 μM 4-OH tamoxifen (Sigma-Aldrich) dissolved in DMSO (Sigma-Aldrich); DMSO-treated cells from the same animal and extraction served as control. In all cell-based experiments, 50 μg/ml ascorbic acid was added fresh every day to ensure proper triple-helical folding of collagens.

Keratinocytes used for cell signaling studies were seeded and grown to subconfluence for 24–48 hours before protein extraction or harvesting of cell medium. For rescue experiments, 12-well plates or coverslips were coated with 15 μg/ml recombinant human COL7A1 in 0.02 N-acetic acid at +4°C, before neutralizing with PBS and seeding of cells.

Western blotting. Proteins were extracted from cultured cells with either RIPA buffer (50 mM Tris–HCl, pH 7.4; 150 mM NaCl; 1% NP-40; 0.5%

sodium deoxycholate; 0.05% SDS; with protease and phosphatase inhibitors, Sigma-Aldrich) or with NP-40 lysis buffer (1% NP-40; 0.1 M NaCl; 0.025 M Tris/HCl, pH 7.4; 10 mM EDTA; with protease and phosphatase inhibitors, Sigma-Aldrich). Protein lysates were separated by SDS–polyacrylamide gel electrophoresis and electroblotted onto nitrocellulose membranes (Bio-Rad). The blots were blocked in milk or BSA, incubated with primary and secondary antibodies in blocking buffer, developed using a Fusion SL system (Peqlab), and quantified with Image J.

Analysis of keratinocyte-conditioned medium. Medium conditioned by confluent keratinocytes was used in order to ensure equivalent conditions in the different groups. Cells were washed 3 times with PBS, and 6 ml keratinocyte medium was added into T25 flasks for 48 hours. The medium was harvested, and 10 mM EDTA and protease inhibitors (Sigma-Aldrich) were added. Medium was chilled to +4°C after harvest, and ammonium sulphate (Sigma-Aldrich) was added to a final concentration of 40%. The medium was precipitated for 1 hour under slow rotation, and the precipitated proteins were pelleted by centrifugation. The pellet dissolved in TBS and the entire pellet was processed and used for Western blotting.

RNA isolation and quantitative polymerase chain reaction. RNA was isolated from cells with NucleoSpin RNA isolation kit (Macherey-Nagel) according to the manufacturer's instructions and transcribed to cDNA with First Strand cDNA Synthesis Kit (Thermo Fisher Scientific). Quantitative real-time polymerase chain reaction analyses were performed with a CFX96 Real-Time system (BioRad). Primers used were as follows: *Gapdh* forward, TTGATGGCAACAATCTCCAC; *Gapdh* reverse, CGTCCCGTAGACAAAATGGT; *Tgfb1* forward, AAGTTGGCATGGTAGCCCTT; *Tgfb1* reverse, GGAGAGCCCTGGATACCAAC; *Fgf2* forward, TGGCACACACTCCCTTGAT; *Fgf2* reverse, AGCGGCTCTACTGCAAGAAC; *Lamb3* forward, TGGAGTCACACTTGCAGCAT; *Lamb3* reverse, CTGTGGGGGACTTGTTCATT.

Immunofluorescence staining. Keratinocytes were grown to subconfluence on coverslips for 24 hours and fixed in acetone and methanol. Skin cryosections were fixed in acetone or 4% PFA. Antigens in paraffin sections were retrieved with sodium citrate or pepsin digestion. Sections were blocked, stained with primary and secondary antibodies, counterstained with DAPI, and mounted in Fluorescence Mounting Medium (Dako). Images were acquired with an Axiocam MRm camera attached to a Zeiss Axio Imager A1 fluorescence microscope (Carl Zeiss), processed using Axiovision 4.8 and ZEN2009 software (Carl Zeiss), and quantified with Image J.

Cell migration assays. 100,000 wild-type or *Col7a1*-hypomorphic murine keratinocytes in passage 3 were seeded to confluence in 35-mm ibidi plates (ibidi) and allowed to attach overnight. The next day, proliferation was stopped with 10 μg/ml mitomycin-C (Sigma-Aldrich). To start migration, the rubber insert was removed, and migration was recorded with a Biostation IM (Nikon). The migrated area was analyzed using Image J.

Wild-type or *Col7a1*-hypomorphic murine fibroblasts were seeded to near confluence in 12-well plates (Nunc) and grown for 2 days in the presence of 50 μg/ml ascorbic acid; on the last day, 5 μg/ml mitomycin-C was added. The monolayers were wounded with a scratch of a 200-μl pipette tip. Photos of the same area were taken 4, 8, 20, and 24 hours after wounding, and wound closure was quantified with Image J.

Fibroblast serum-response assay. Fibroblast serum-response experiments were performed as described previously (26), with minor modifications. Briefly, murine fibroblasts in passage 2 were seeded in 6-well plates (Nunc) with DMEM/F12 and 10% FCS and allowed to attach overnight. Next, cells were washed with D-PBS and starved with 0.1% DMEM/F12 for 48 hours. Cells were subsequently stimulated for 5 hours with either 10% FCS or 0.1% FCS, and RNA was isolated. For "rescue" experiments, the wells of a 24-well plate (Nunc) were coated with 100 μl of 15 μg/ml rat tail collagen I in 0.02 N-acetic acid or with 100 μl of a mixture of 15 μg/ml recombinant human COL7A1 and 15 μg/ml rat tail collagen I in 0.02 N-acetic acid.

Human skin specimens. Biopsy specimens of acute wounds were derived from re-excision of wound margins 3 days after primary excision of a skin lesion. Chronic wound specimens were from diagnostic biopsies from the wound margins of nonhealing leg ulcers due to chronic venous insufficiency. RDEB wound biopsy specimens were obtained from *COL7A1*-deficient patients with severe generalized RDEB.

Statistics. Statistical analysis was performed with GraphPad Prism 5.03 software (GraphPad Software) using unpaired or paired 2-tailed Student's *t* test as appropriate. A P value less than 0.05 was considered statistically significant.

Study approval. All animal experiments were approved by the regional review board (Regierungspräsidium Freiburg, Freiburg, Germany; approval no. 35/9185.81/G09-80). Studies using patient material were approved by the Ethics Committee of the University of Freiburg (approval no. G09/080) and conducted according to the Declaration of Helsinki. Patients provided informed consent prior to their participation.

Further information can be found in the article supplement (55, 56).

Acknowledgments

This work was supported by the Excellence Initiative of the German Federal and State Governments through the Freiburg Institute for Advanced Studies (FRIAS), by School of Life Sciences — LifeNet, by grants SI 1281/2-1 and BR 1475/12-1 from the German Research Foundation (DFG), by grant BMBF 016N0971 from the German Ministry for Education and Research (BMBF), and by Debra International (Bruckner-Tuderman 4 and Bruckner-Tuderman/Handgretinger 1). A. Nyström was supported by a grant from BMBF under the frame of Erare-2, the ERA-Net for Research on Rare Diseases. We thank Reinhard Fässler (Max Planck Institute of Biochemistry, Martinsried, Germany) for help with generation of the transgenic mice, Ingrid Hausser (University of Heidelberg) for electron microscopy, Sylke Lange for excellent technical assistance, and Kim Yancey and Lydia Sorokin for providing antibodies.

Received for publication December 3, 2012, and accepted in revised form May 9, 2013.

Address correspondence to: Leena Bruckner-Tuderman, Department of Dermatology, Freiburg University Medical Center, Hauptstr. 7, Freiburg 79104, Germany. Phone: 49.761.270.67160; Fax: 49.761.270.69360; E-mail: bruckner-tuderman@uniklinik-freiburg.de.

1. Coulombe PA. Wound epithelialization: accelerating the pace of discovery. *J Invest Dermatol*. 2003; 121(2):219–230.
2. Singer AJ, Clark RA. Cutaneous wound healing. *N Engl J Med*. 1999;341(10):738–746.
3. Schäfer M, Werner S. Cancer as an overhealing wound: an old hypothesis revisited. *Nat Rev Mol Cell Biol*. 2008;9(8):628–638.
4. Werner S, Grose R. Regulation of wound healing by growth factors and cytokines. *Physiol Rev*. 2003; 83(3):835–870.
5. Ko MS, Marinkovich MP. Role of dermal-epidermal basement membrane zone in skin, cancer, and developmental disorders. *Dermatol Clin*. 2010; 28(1):1–16.
6. Bruckner-Tuderman L, Höpfner B, Hammami-Hauasli N. Biology of anchoring fibrils: lessons from dystrophic epidermolysis bullosa. *Matrix Biol*. 1999; 18(1):43–54.
7. Bruckner-Tuderman L. European Dermatology Forum: skin diseases in Europe. Skin diseases with a high public health impact: Epidermolysis bullosa. *Eur J Dermatol*. 2008;18(2):214–216.
8. Tsuruta D, Hashimoto T, Hamill KJ, Jones JC. Hemidesmosomes and focal contact proteins: functions and cross-talk in keratinocytes, bullous diseases and wound healing. *J Dermatol Sci*. 2011;62(1):1–7.
9. Sehgal BU, et al. Integrin beta4 regulates migratory behavior of keratinocytes by determining laminin-332 organization. *J Biol Chem*. 2006;281(46):35487–35498.
10. Pullar CE, et al. beta4 integrin and epidermal growth factor coordinately regulate electric field-mediated directional migration via Rac1. *Mol Biol Cell*. 2006;17(11):4925–4935.
11. Goldfinger LE, Stack MS, Jones JC. Processing of laminin-5 and its functional consequences: role

of plasmin and tissue-type plasminogen activator. *J Cell Biol*. 1998;141(1):255–265.
12. Kligys K, et al. The slingshot family of phosphatases mediates Rac1 regulation of cofilin phosphorylation, laminin-332 organization, and motility behavior of keratinocytes. *J Biol Chem*. 2007; 282(44):32520–32528.
13. Sakai LY, Keene DR, Morris NP, Burgeson RE. Type VII collagen is a major structural component of anchoring fibrils. *J Cell Biol*. 1986;103(4):1577–1586.
14. Van Agtmael T, Bruckner-Tuderman L. Basement membranes and human disease. *Cell Tissue Res*. 2010;339(1):167–188.
15. Intong LR, Murrell DF. Inherited epidermolysis bullosa: new diagnostic criteria and classification. *Clin Dermatol*. 2012;30(1):70–77.
16. Varki R, Sadowski S, Uitto J, Pfendner E. Epidermolysis bullosa. II. Type VII collagen mutations and phenotype-genotype correlations in the dystrophic subtypes. *J Med Genet*. 2007;44(3):181–192.
17. Bruckner-Tuderman L. Dystrophic epidermolysis bullosa: pathogenesis and clinical features. *Dermatol Clin*. 2010;28(1):107–114.
18. Fine JD, et al. The classification of inherited epidermolysis bullosa (EB): Report of the Third International Consensus Meeting on Diagnosis and Classification of EB. *J Am Acad Dermatol*. 2008; 58(6):931–950.
19. Tolar J, Blazar BR, Wagner JE. Concise review: Transplantation of human hematopoietic cells for extracellular matrix protein deficiency in epidermolysis bullosa. *Stem Cells*. 2011;29(6):900–906.
20. Woodley DT, et al. Intravenously injected human fibroblasts home to skin wounds, deliver type VII collagen, and promote wound healing. *Mol Ther*. 2007;15(3):628–635.
21. Conget P, et al. Replenishment of type VII collagen and re-epithelialization of chronically ulcerated skin after intradermal administration of allogeneic mesenchymal stromal cells in two patients with recessive dystrophic epidermolysis bullosa. *Cytotherapy*. 2010;12(3):429–431.
22. Fritsch A, et al. A hypomorphic mouse model of dystrophic epidermolysis bullosa reveals mechanisms of disease and response to fibroblast therapy. *J Clin Invest*. 2008;118(5):1669–1679.
23. Guo W, et al. Beta 4 integrin amplifies ErbB2 signaling to promote mammary tumorigenesis. *Cell*. 2006;126(3):489–502.
24. Nikolopoulos SN, et al. Targeted deletion of the integrin beta4 signaling domain suppresses laminin-5-dependent nuclear entry of mitogen-activated protein kinases and NF-kappaB, causing defects in epidermal growth and migration. *Mol Cell Biol*. 2005;25(14):6090–6102.
25. Waterman EA, et al. A laminin-collagen complex drives human epidermal carcinogenesis through phosphoinositol-3-kinase activation. *Cancer Res*. 2007;67(9):4264–4270.
26. Iyer VR, et al. The transcriptional program in the response of human fibroblasts to serum. *Science*. 1999;283(5398):83–87.
27. Leask A, Abraham DJ. TGF-beta signaling and the fibrotic response. *FASEB J*. 2004;18(7):816–827.
28. Woodley DT, Hou Y, Martin S, Li W, Chen M. Characterization of molecular mechanisms underlying mutations in dystrophic epidermolysis bullosa using site-directed mutagenesis. *J Biol Chem*. 2008;283(26):17838–17845.
29. Martins VL, et al. Increased invasive behaviour in cutaneous squamous cell carcinoma with loss of basement-membrane type VII collagen. *J Cell Sci*. 2009;122(pt 11):1788–1799.
30. Frank DE, Carter WG. Laminin 5 deposition regulates keratinocyte polarization and persistent migration. *J Cell Sci*. 2004;117(pt 8):1351–1363.
31. Zhang Z, et al. Migration of epithelial cells on laminins: RhoA antagonizes directionally persistent migration. *Eur J Cell Biol*. 2011;90(1):1–12.
32. Sullivan SR, et al. Topical application of laminin-332 to diabetic mouse wounds. *J Dermatol Sci*. 2007;48(3):177–188.
33. Margadant C, Raymond K, Kreft M, Sachs N, Janssen H, Sonnenberg A. Integrin alpha3beta1 inhibits directional migration and wound re-epithelialization in the skin. *J Cell Sci*. 2009;122(pt 2):278–288.
34. O'Toole EA, Marinkovich MP, Hoeffler WK, Furthmayr H, Woodley DT. Laminin-5 inhibits human keratinocyte migration. *Exp Cell Res*. 1997; 233(2):330–339.
35. Kariya Y, Sato H, Katou N, Kariya Y, Miyazaki K. Polymerized laminin-332 matrix supports rapid and tight adhesion of keratinocytes, suppressing cell migration. *PLoS One*. 2012;7(5):e35546.
36. Raymond K, Kreft M, Janssen H, Calafat J, Sonnenberg A. Keratinocytes display normal proliferation, survival and differentiation in conditional beta4-integrin knockout mice. *J Cell Sci*. 2005; 118(pt 5):1045–1060.
37. Hintermann E, Bilban M, Sharabi A, Quaranta V. Inhibitory role of alpha 6 beta 4-associated erbB-2 and phosphoinositide 3-kinase in keratinocyte haptotactic migration dependent on alpha 3 beta 1 integrin. *J Cell Biol*. 2001;153(3):465–478.
38. Hintermann E, Yang N, O'Sullivan D, Higgins JM, Quaranta V. Integrin alpha6beta4-erbB2 complex inhibits haptotaxis by up-regulating E-cadherin cell-cell junctions in keratinocytes. *J Biol Chem*. 2005; 280(9):8004–8015.
39. Owens DM, Romero MR, Gardner C, Watt FM. Suprabasal alpha6beta4 integrin expression in epidermis results in enhanced tumourigenesis and disruption of TGFbeta signalling. *J Cell Sci*. 2003; 116(pt 18):3783–3791.
40. Chen M, O'Toole EA, Li YY, Woodley DT. Alpha 2 beta 1 integrin mediates dermal fibroblast attachment to type VII collagen via a 158-amino-acid segment of the NC1 domain. *Exp Cell Res*. 1999; 249(2):231–239.
41. Chen M, Costa FK, Lindvay CR, Han YP, Woodley DT. The recombinant expression of full-length type VII collagen and characterization of molecular mechanisms underlying dystrophic epidermolysis bullosa. *J Biol Chem*. 2002;277(3):2118–2124.
42. Woodall BP, et al. Integrin alpha2beta1 is the required receptor for endorepellin angiostatic activity. *J Biol Chem*. 2008;283(4):2335–2343.
43. Ng YZ, et al. Fibroblast-derived dermal matrix drives development of aggressive cutaneous squamous cell carcinoma in patients with recessive dystrophic epidermolysis bullosa. *Cancer Res*. 2012; 72(14):3522–3534.
44. Järvinen TA, Ruoslahti E. Target-seeking antifibrotic compound enhances wound healing and suppresses scar formation in mice. *Proc Natl Acad Sci U S A*. 2010;107(50):21671–21676.
45. Han G, Wang XJ. Roles of TGFbeta signaling Smads in squamous cell carcinoma. *Cell Biosci*. 2011;1:41.
46. Hinz B. The myofibroblast: paradigm for a mechanically active cell. *J Biomech*. 2010;43(1):146–155.
47. Wells RG, Discher DE. Matrix elasticity, cytoskeletal tension, and TGF-beta: the insoluble and soluble meet. *Sci Signal*. 2008;1(10):pe13.
48. Wipff PJ, Rifkin DB, Meister JJ, Hinz B. Myofibroblast contraction activates latent TGF-beta1 from the extracellular matrix. *J Cell Biol*. 2007; 179(6):1311–1323.
49. Evans RA, Tian YC, Steadman R, Phillips AO. TGF-beta1-mediated fibroblast-myofibroblast terminal differentiation-the role of Smad proteins. *Exp Cell Res*. 2003;282(2):90–100.
50. Cowin AJ, et al. Flightless I deficiency enhances wound repair by increasing cell migration and proliferation. *J Pathol*. 2007;211(5):572–581.
51. Kopecki Z, et al. Overexpression of the Flii gene increases dermal-epidermal blistering in an autoimmune ColVII mouse model of epidermolysis bullosa acquisita. *J Pathol*. 2011;225(3):401–413.
52. Fritsch A, et al. Dominant-negative effects of COL7A1 mutations can be rescued by controlled overexpression of normal collagen VII. *J Biol Chem*. 2009;284(44):30248–30256.
53. Kern JS, et al. Mechanisms of fibroblast cell therapy for dystrophic epidermolysis bullosa: high stability of collagen VII favors long-term skin integrity. *Mol Ther*. 2009;17(9):1605–1615.
54. Franzke CW, et al. Epidermal ADAM17 maintains the skin barrier by regulating EGFR ligand-dependent terminal keratinocyte differentiation. *J Exp Med*. 2012;209(6):1105–1119.
55. Larjava H, Salo T, Haapasalmi K, Kramer RH, Heino J. Expression of integrins and basement membrane components by wound keratinocytes. *J Clin Invest*. 1993;92(3):1425–1435.
56. Schéele S, Nyström A, Durbeej M, Talts JF, Ekblom M, Ekblom P. Laminin isoforms in development and disease. *J Mol Med (Berl)*. 2007;85(8):825–836.